Amino Acids

A dynamic model for the p53 stress response networks under ion radiation

J.-P. Qi [1], **S.-H. Shao** [1], **D.-D. Li** [1], and **G.-P. Zhou** [2]

[1] Bio-Informatics Research Center, Donghua University, Shanghai, China
[2] Department of Biological Chemistry and Molecular Pharmacology, Harvard Medical School, Boston, MA, U.S.A.

Summary. P53 controls the cell cycle arrest and cell apoptosis through interaction with the downstream genes and their signal pathways. To stimulate the investigation into the complicated responses of p53 under the circumstance of ion radiation (IR) in the cellular level, a dynamic model for the p53 stress response networks is proposed. The model can be successfully used to simulate the dynamic processes of generating the double-strand breaks (DSBs) and their repairing, ataxia telangiectasia mutated (ATM) activation, as well as the oscillations occurring in the p53-MDM2 feedback loop.

Keywords: Cellular networks – p53 – MDM2 – IR – DNA damage – Oscillations

1. Introduction

As a vital anticancer gene, p53 can regulate its downstream genes through their signal pathways, and further implement cell cycle arrest and cell apoptosis (Chou et al., 1999a, 2000; Perez and Purdy, 1998; Vogelstein et al., 2000). These functions are important to repair DNA damage, and eliminate the abnormal cells with DNA damage or deregulated proliferation, especially to modulate the activity of anticancer agents (Chou et al., 1997; Pauklin et al., 2005; Ritter et al., 2002).

Recently, several models have been proposed to explain the damped oscillations of p53 in cell populations (Lev Bar-Or et al., 2000; Ma et al., 2005). However, the dynamic mechanism of the single-cell responses is not completely clear yet, and the complicated regulations among genes and their signal pathways need to be further addressed. Based on the previous models (Lev Bar-Or et al., 2000; Ma et al., 2005) and stimulated by the impact of the bioinformatical approaches on the biomedicine (Chou, 2004), a dynamic model for the p53 stress response networks under IR was proposed, along with the kinetics

of DSB generation and repair, ATM activation, as well as the p53-MDM2 feedback loop module. Furthermore, analyses were given on the threshold time for the switch-like ATM activation, as well as on the number and amplitude of oscillations between p53 and MDM2 in response to IR.

Using differential equations and graphic approaches to study various dynamical and kinetic processes of biological systems can provide useful insights, as indicated by many previous studies on a series of important biological topics, such as enzyme-catalyzed reactions (Chou, 1989a; Chou and Forsen, 1980; Chou et al., 1979; King and Altman, 1956; Kuzmic et al., 1992; Lin and Neet, 1990; Zhou and Deng, 1984), internal motions of biomacromolecules (Chou, 1984, 1987, 1988, 1989b; Chou and Chen, 1977; Chou et al., 1989; Chou and Mao, 1988; Han, 1992; Han and Wang, 1992; Martel, 1992; Sobell et al., 1983), diffusion-controlled reactions in enzyme systems (Chou and Jiang, 1974; Chou and Zhou, 1982; Cotes and Sceats, 1988; Zhou et al., 1983; Zhou and Zhong, 1982), protein folding kinetics (Chou, 1990), inhibition kinetics of processive nucleic acid polymerases and nucleases (Althaus et al., 1993a, b; Chou et al., 1994a), soliton transport in protein and DNA (Chou et al., 1994b; Sinkala, 2006; Zhou, 1989), analysis of codon usage (Chou and Zhang, 1992; Zhang and Chou, 1994), base frequencies in the anti-sense strands (Zhang and Chou, 1996), hepatitis B viral infections (Xiao et al., 2006), HBV virus gene missense mutation (Xiao et al., 2005), and visual analysis of SARS-CoV (Gao et al., 2006; Wang et al., 2005). In this study, we used differential equations and graphic methods to investigate the dynamic and kinetic processes of p53 stress response networks under the effects of IR.
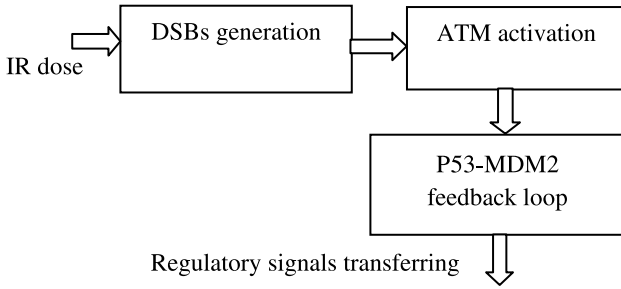
Fig. 1. Integrated model of p53 stress response networks under IR, composed of DSBs generation and repair, ATM activation, and p53-MDM2 feedback regulation

Fig. 2. DSBs generation and repair module. DSBs induced by IR can be in one of three states: intact DSB, DBSC, and fixed DSBs (F_d), subscripts '1' and '2' differentiate the fast kinetics and the slow kinetics

2. Model of P53 stress response networks

Under the genome stresses, numerous co-factors are involved in enhancing p53-mediated transcription (Magne et al., 2006). The interactions among these co-factors make the model more complicated. Therefore, some simplification procedures are needed in order to allow the model to incorporate more biochemical information (Tyson, 1999; Tyson and Novak, 2001). To realize this, let us take the following criteria or assumptions: (1) only the vital components and interactions are taken into account in the model; (2) all the localization issues are ignored; (3) the simple linear relations are used to describe the interactions among the components concerned; and (4) there are enough substances to keep the system "workable" (Tyson, 1999).

The scheme of the integrated model is given in Fig. 1. In the DSBs generation and repair module, the acute IR induces DSBs stochastically and forms DSB-protein complexes (DSBCs) at each of the damage sites after interacting with the DNA repair proteins. As a sensor of genome stress, ATM is activated by the DSBCs signal transferred from DSBs. ATM activation switches on or off the p53-Mdm2 feedback loop, further regulating the downstream genes to control the cell cycle arrest and the cell apoptosis in response to genome stresses (Weller, 1998).

2.1 DSBs generation and repair module

Under the continuous effect of acute IR dose, DSBs occur and trigger two major repair mechanisms in eukaryotic cells: homologous recombination (HR) and nonhomologous end joining (NHEJ) (Rapp and Greulich, 2004; Rothkamm et al., 2003). DSB repair is a first-order process if the break ends associated with the same DSB are rejoined, or a second-order process if the break ends associated with two different DSBs are rejoined (Daboussi
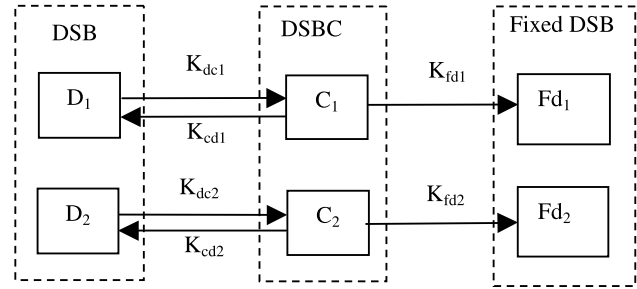
et al., 2002). Meanwhile, about 60–80% of DSBs are rejoined quickly, whereas the remaining 20–40% of DSBs are rejoined more slowly (Budman and Chu, 2005; Daboussi et al., 2002).

In the first part of our model, we implement the module of DSBs generation and repair process. As shown in Fig. 2, the module contains both the fast and slow kinetics, each is composed of a reversible binding of repair proteins and DSB lesions into DSBCs, and an irreversible process from the DSBCs to the fixed DSBs (Daboussi et al., 2002; Rapp and Greulich, 2004).

Some experimental data suggest that the quantity of the resulting DSBs within different IR dose domains obey a Poisson distribution (Ma et al., 2005). In accordance with the experiments, we assume that the stochastic number of the resulting DSBs per time scale is proportional to the number generated by a Poisson random function during the period of acute radiation (Ma et al., 2005). The DSBs generation process is formulated as follows:

$$\frac{d[D_T]}{dt} = k_T \times \text{Poissrnd}(a_{ir} \times \text{IR}) \tag{1}$$

where $[D_T]$ is the concentration of the total resulting DSBs induced by continuous IR in both fast and slow repair process, k_T the parameter to set the number of DSBs per time scale, and a_{ir} the parameter to set the number of DSBs per IR dose.

Moreover, we assume that adequate repair proteins are available around DSBs sites, and 70% of the initial DSBs are fixed by the fast repair process. Each DSB can be in one of the following three states: intact DSB, DSBC, and fixed DSB. Thus, we have the following differential equations:

$$\frac{d[D_1]}{dt} = a_1[D_T] + k_{cd1}[C_1] - (k_{dc1}[D_1] + k_{cross}([D_1] + [D_2])) \tag{2}$$

$$\frac{d[D_2]}{dt} = a_2[D_T] + k_{cd2}[C_2] - (k_{dc2}[D_2]$$
$$+ k_{cross}([D_1] + [D_2])) \tag{3}$$

$$\frac{d[C_1]}{dt} = k_{dc1}[D_1] - k_{cd1}[C_1] - k_{cf1}[C_1] \tag{4}$$

$$\frac{d[C_2]}{dt} = k_{dc2}[D_2] - k_{cd2}[C_2] - k_{cf2}[C_2] \tag{5}$$

$$\frac{d[F_d]}{dt} = k_{fd1}[C_1] + k_{fd2}[C_2] \tag{6}$$

where $[D]$, $[C]$, and $[F_d]$ represent the respective concentrations of DSB, DSBC, and fixed DSB; k_{dc}, k_{cd}, k_{fd} are the transition rates among the above three states; k_{dc}, and k_{cross} represent the repair rates of the first-order and the second-order process (Daboussi et al., 2002), and the subscripts '1' and '2' refer to the fast and the slow kinetics.

2.2 ATM activation module

As a DNA damage detector, ATM exists as a dimer in unstressed cells. After IR is applied, intermolecular autophosphorylation occurs, causing the dimer to dissociate rapidly into the active monomers. The active ATM monomer (ATM*) can prompt the p53 expression further (Budman and Chu, 2005; Daboussi et al., 2002). Like (Chou et al., 1999b), here we use the superscript $*$ to represent the activate state. Based on the existing model of ATM switch (Ma et al., 2005), we present an ATM activation module under IR. Figure 3 shows the module scheme, which includes three components: ATM dimer, inactive ATM monomer, and ATM*. Here, we assume that DSBCs is the main signal transduction from DSBs to p53-MDM2 feedback loop through ATM activation, and the rate of ATM activation is a function of the amount of DSBCs and the self-feedback of ATM*. Furthermore, the total concentration of ATM is a constant, including ATM dimer, ATM monomer and ATM* (Ma et al., 2005).

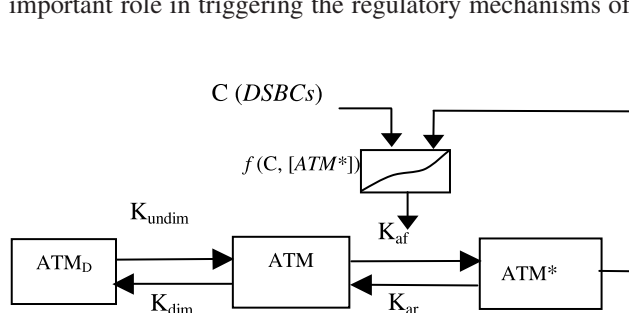As a detector of DNA damage, ATM activation plays an important role in triggering the regulatory mechanisms of

p53 stress response networks (Kohn and Pommier, 2005; Oren, 2003). After the acute IR is applied, phosphorylation of inactive ATM monomers is promoted first by DSBCs and then rapidly by means of the positive feedback from ATM*, accounting for the intermolecular autophosphorylation (Ma et al., 2005). The main formulations are as follows:

$$\frac{d[ATM_d]}{dt} = \frac{1}{2}k_{dim}[ATM]^2 - k_{undim}[ATM_d] \tag{7}$$

$$\frac{d[ATM]}{dt} = 2k_{undim}[ATM_d] - k_{dim}[ATM]^2$$
$$- k_{af}f[ATM] + k_{ar}[ATM^*] \tag{8}$$

$$\frac{d[ATM^*]}{dt} = k_{af}f[ATM] - k_{ar}[ATM^*] \tag{9}$$

$$f(C, [ATM^*]) = a_1C + a_2[ATM^*] + a_3C[ATM^*] \tag{10}$$

where $[ATM_d]$, $[ATM]$ and $[ATM^*]$ represent the concentrations of ATM dimer, ATM monomer, and active ATM monomer respectively; k_{undim} is the rate of ATM undimerization, and k_{dim} the rate of ATM dimerization; k_{ar} is the rate of ATM monomer inactivation, and k_{af} the rate of ATM monomer activation. In addition, f is the function of ATM activation, the term a_1C implies the fact that DSBs somehow activate ATM molecules at a distance, $a_2[ATM^*]$ indicates the mechanism of autophosphorylation of ATM, and $a_3C[ATM^*]$ represents the interaction between the DSBCs and ATM* (Bakkenist and Kastan, 2003; Ma et al., 2005).

2.3 P53-MDM2 feedback loop module

As shown in Fig. 4, p53 and its principal antagonist, Mdm2 is transactivated by p53, form a p53-MDM2 feedback loop. ATM* can elevates the transcriptional activity of p53 by prompting phosphorylation of p53 and degradation of MDM2 protein (Lev Bar-Or et al., 2000).
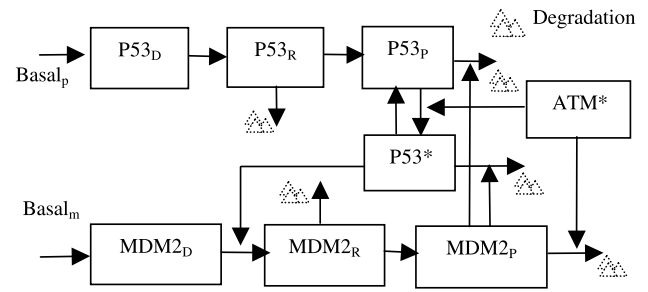

Fig. 4. The module of p53-MDM2 feedback loop. ATM* elevates the transcriptional activity of p53 by prompting phosphorylation of p53 and degradation of MDM2 protein, the increase of Mdm2 proteins promote a fast degradation of p53 and a slow degradation of p53*

Fig. 3. The module of ATM activation under IR. With the cooperation of DSBCs and self-feedback of ATM*, ATM is activated from ATM monomers under the continuous IR

This negative feedback loop can produce oscillations in response to the sufficiently strong IR dose (Ma et al., 2005).

To account for a decreased binding affinity between inactive p53 and p53*, we assume that MDM2-induced degradation of inactive p53 is faster than that of p53*. The main differential equations used in this module are as follows:

$$\frac{d[\text{P53}_\text{R}]}{dt} = S_{\text{P53}} - d_{\text{rp}}[\text{P53}_\text{R}] - k_{\text{rp}}[\text{P53}_\text{R}] \tag{11}$$

$$\frac{d[\text{P53}_\text{P}]}{dt} = k_{\text{rp}}[\text{P53}_\text{R}] + k_{\text{p*p}}[\text{P53}^*]$$
$$- d_{\text{pp}}[\text{P53}_\text{P}] - k_{\text{app*}}[\text{ATM}^*]\frac{[\text{P53}_\text{P}]}{[\text{P53}_\text{P}] + k_{\text{p}}}$$
$$- k_{\text{mp}}[\text{MDM2}_\text{P}]\frac{[\text{P53}_\text{P}]}{[\text{P53}_\text{P}] + k_{\text{d}}} \tag{12}$$

$$\frac{d[\text{P53}^*]}{dt} = k_{\text{app*}}[\text{ATM}^*]\frac{[\text{P53}_\text{P}]}{[\text{P53}_\text{P}] + k_{\text{p}}}$$
$$- k_{\text{p*p}}[\text{P53}^*] - d_{\text{pp*}}[\text{P53}^*]$$
$$- k_{\text{mp*}}[\text{MDM2}_\text{P}]\frac{[\text{P53}^*]}{[\text{P53}^*] + k_{\text{d*}}} \tag{13}$$

$$\frac{d[\text{MDM2}_\text{R}]}{dt} = S_{\text{mdm2}} + k_{\text{p*m}}\frac{[\text{P53}^*]^n}{[\text{P53}^*]^n + k^n}$$
$$- k_{\text{mrp}}[\text{MDM2}_\text{R}] - d_{\text{mr}}[\text{MDM2}_\text{R}] \tag{14}$$

$$\frac{d[\text{MDM2}_\text{P}]}{dt} = k_{\text{mrp}}[\text{MDM2}_\text{R}] - d_{\text{mp}}[\text{MDM2}_\text{P}]$$
$$- k_{\text{mat}}\frac{[\text{ATM}^*]}{[\text{ATM}^*] + k_{\text{at}}}[\text{MDM2}_\text{p}] \tag{15}$$

where $[\text{P53}_\text{R}]$, $[\text{P53}_\text{P}]$, $[\text{P53}^*]$, $[\text{MDM2}_\text{R}]$, and $[\text{MDM2}_\text{P}]$ represent the concentrations of p53 mRNA, p53 protein and active p53, MDM2 mRNA, and MDM2 protein, respectively. S_{p53}, S_{MDM2} are the basal induction rate of p53 mRNA, and that of MDM2 mRNA. The other parameters are presented in Tables 1–3.

Table 1. Parameters used in the module of DSBs generation and repair process

Parameters	Description	Constant
k_t	Rate of DSBs generation per time scale	0.01
a_ir	Number of DSBs generation per IR dose	35
a_1	Percentage of DSBs processed by fast repair	0.70
a_2	Percentage of DSBs processed by slow repair	0.30
k_dc1	Rate of DSBs transition to DSBCs in fast repair process	2
k_dc2	Rate of DSBs transition to DSBCs in slow repair process	0.2
k_dc1	Rate of DSBCs transition to DSBs in fast repair process	0.5
k_dc2	Rate of DSBCs transition to DSBs in slow repair process	0.05
k_fd1	Rate of DSCs transition to F_d in fast repair process	0.001
k_fd2	Rate of DSCs transition to F_d in slow repair process	0.0001
k_cross	Rate of DSB binary mismatch in second order repair process	0.001

Table 2. Parameters used in the module of ATM activation process

Parameters	Description	Constant
k_dim	ATM dimerization rate	8
k_undim	ATM undimerization rate	1
K_af	ATM phosphorylation rate	1
K_ar	ATM dephosphorylation rate	3
a_1	Scale of the activation function of ATM phosphorylation	1
a_2	Scale of the activation function of ATM phosphorylation	0.08
a_3	Scale of the activation function of ATM phosphorylation	0.8

Table 3. Parameters used in the module of p53-MDM2 feedback regulatory loop

Parameters	Description	Constant
S_p53	Basal induction rate of p53 mRNA	0.001
d_rp	Degradation rate of p53 mRNA	0.02
k_rp	Translation rate of *p53* mRNA	0.12
$k_\text{p*p}$	Dephosphorylation rate of p53*	0.2
$k_\text{app*}$	ATM*-dependent phosphorylation rate of p53	0.6
k_mp	Mdm2-dependent degradation rate of p53	0.1
$k_\text{mp*}$	Mdm2-dependent degradation rate of p53*	0.02
d_pp	Basal degradation rate of p53	0.02
$d_\text{pp*}$	Basal degradation rate of p53*	0.008
S_mdm2	Basal induction rate of *MDM2* mRNA	0.002
$k_\text{p*m}$	P53-dependent *Mdm2* transcription rate	0.03
k_mrp	Translation rate of *Mdm2* mRNA	0.02
d_mr	Degradation rate of *Mdm2* mRNA	0.01
d_mp	Basal degradation rate of *Mdm2*	0.003
k_mat	ATM*-dependent degradation rate of *Mdm2*	0.01
k_p	Michaelis constant of ATM*-dependent *p53* phosphorylation	1.0
k	Michaelis constant of p53-dependent *Mdm2* transcription	1.0
k_d	Threshold concentration for Mdm2-dependent p53 degradation	0.03
n	Hill coefficient of *Mdm2* transcription rate	4
k_at	Threshold concentration for ATM*-dependent *Mdm2* degradation	1.60
$k_\text{d*}$	Threshold concentration for Mdm2-dependent *p53* degradation	0.32

3. Simulation results

To ensure the accuracy of the simulation results, let us consider the fact that the valid parameter sets should obey the following rules (Kohn and Pommier, 2005; Lev Bar-Or et al., 2000; Ma et al., 2005): (1) the model must contain oscillations. This is important as there has been experimental evidence that oscillations occur between p53 and MDM2 after cell stress; (2) the mechanism used to mathematically describe the degradation of p53 by MDM2 is accurate only for low concentrations of p53; (3) the concentration of p53* is much higher than that of inactive p53 after the system reaching an equilibrium. Based on these three rules and the existing parameter sets used in (Ma et al., 2005), we obtained the kinetics of p53 stress response networks under acute IR dose through

simulation platform in MATLAB7.0. The detailed parameter sets used in our model can be found in Tables 1–3.

3.1 DNA damage generation and repair process

During the simulation process, we applied 8 Gy IR to generate DSBs fraction. In order to agree with the experimental results that the measured 30–40 DSBs per Gy occurred in the single cell (Ma et al., 2005), the stochastic number of resulting DSBs were generated by using a Poisson random function with a mean of $35x$ as continuous IR dose of x Gy was applied. Figure 5a displays a stochastic trace of the resulting DSBs versus the constant radiation time.

Compared with the Monte Carlo methods (Ma et al., 2005), our simulation method is more suitable for the
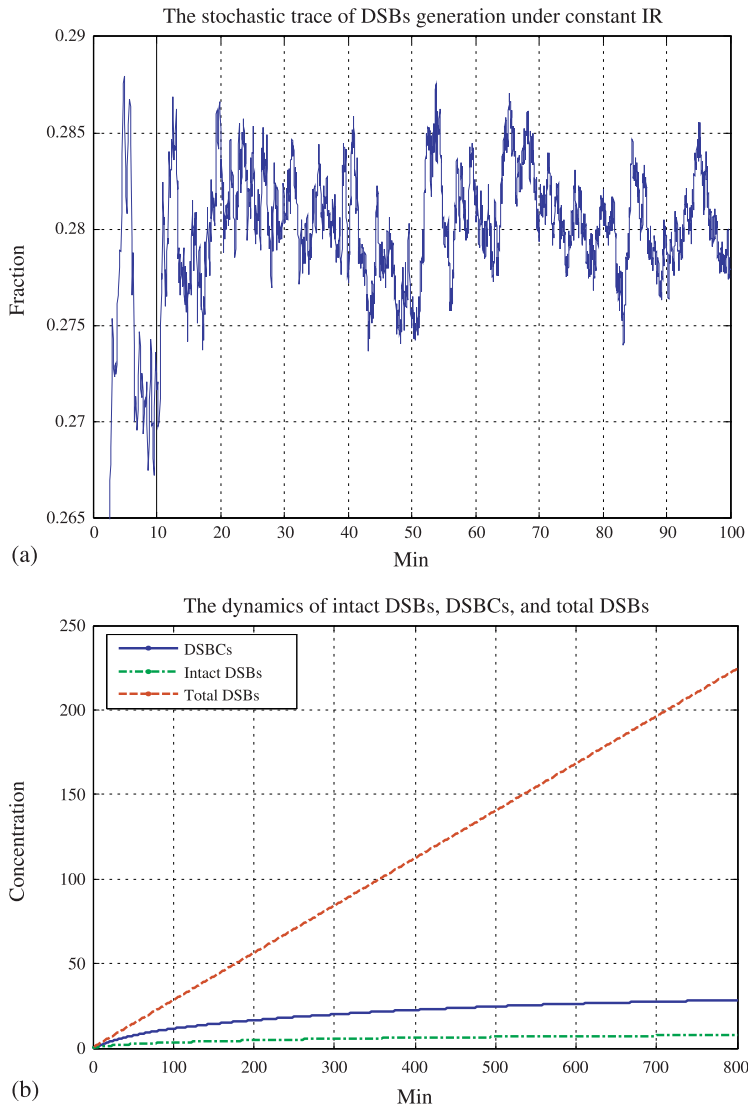

(a)

(b)

Fig. 5. The kinetics of DSBs generation and repair process under IR = 8 Gy. **a** Stochastic trace of DSBs generation induced by continuous IR; **b** Dynamic relationships among intact DSBs, DSBCs and resulting DSBs

conditions with the presence of many resulting DSBs and adequate repair proteins in the cell. Meanwhile, the simulation results can describe the stochastic kinetics of DSBs generation under the continuous effects of the acute IR. Figure 5b shows the dynamic traces of resulting DSBs, DSBCs, and intact DSBs in response to 8 Gy IR in both fast and slow repair kinetics.

3.2 ATM activation

The ATM activation module was established to describe the switch-like dynamics of the ATM activation in response to DSBCs increasing, and the regulation mechanisms during the process of the ATM transferring DNA damage signals to the p53-MDM2 feedback loop. Under the cooperative function of DSBCs and the positive self-feedback of ATM*, the ATM would reach the equilibrium state within minutes because of the fast phosphor-

ylation (Ma et al., 2005). As shown in Fig. 6a, the concentration of ATM* increases fast against the decreasing of ATM dimer and ATM monomer, both of which reach the cross point behind the IR by about 9 minutes. In Fig. 6b delineates the kinetic process of ATM* versus IR dose increasing, and the process of ATM reaching the saturation after IR overpass the threshold value by about 0.5 Gy.

The immunoblot studies (Bakkenist and Kastan, 2003) show a rather abrupt onset of activated ATM that starts at 0.1–0.2 Gy and reaches saturation at about 0.4 Gy. The step-like traces in Fig. 6a suggest that the ATM module can produce an on-off switching signal to the p53-MDM2 feedback loop; the simulation shown in Fig. 6b qualitatively resembles the results in (Bakkenist and Kastan, 2003; Ma et al., 2005) and the actual data reported in (Bakkenist and Kastan, 2003) except for the saturation at about 0.5 Gy.
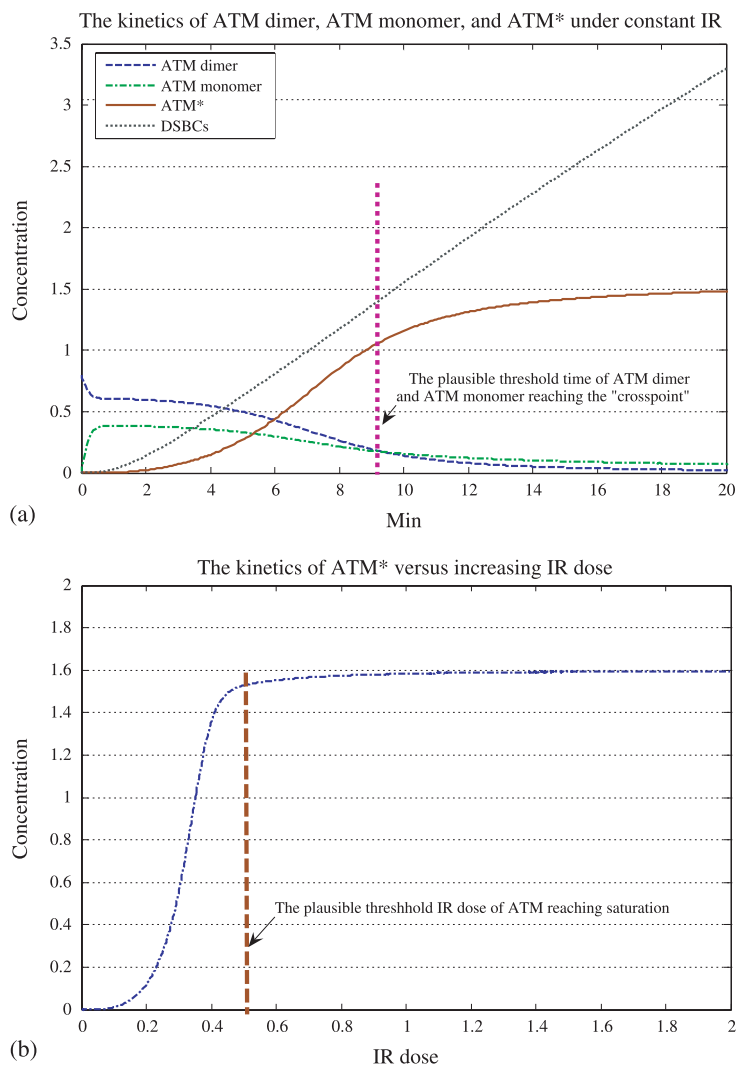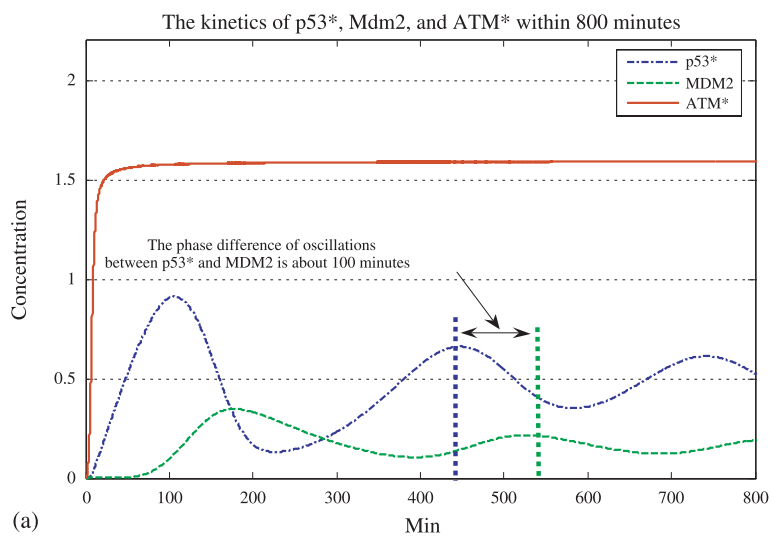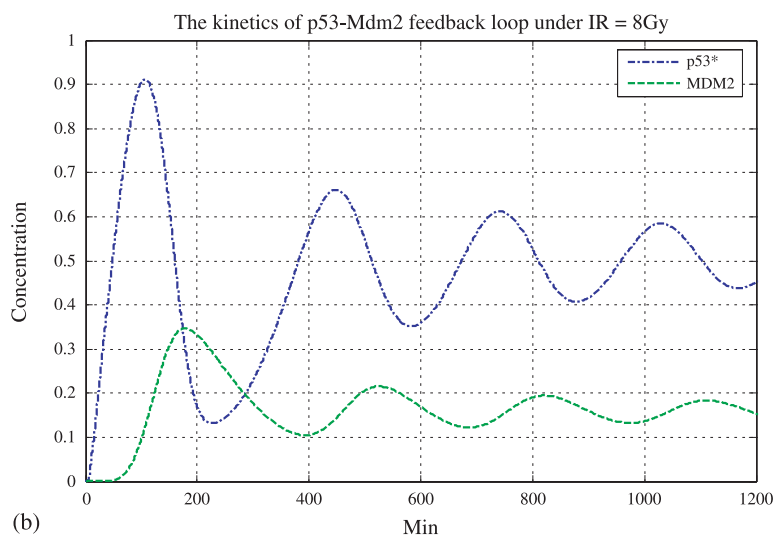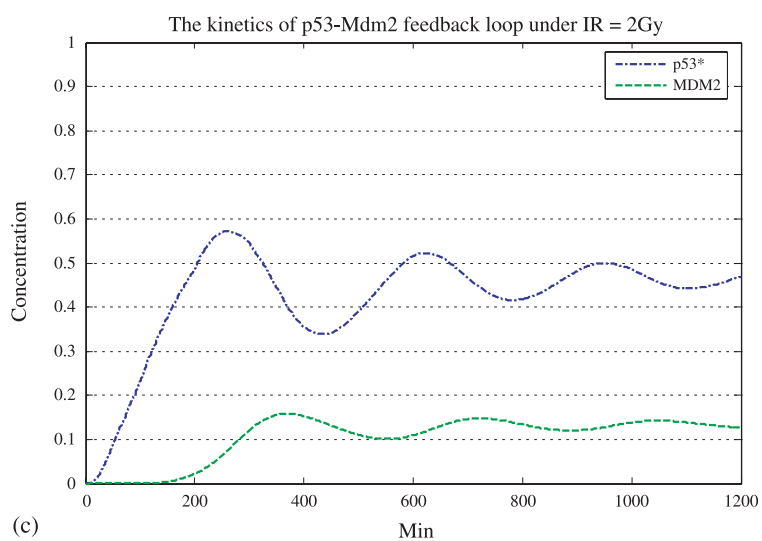

(a)

(b)

Fig. 6. The dynamics of ATM activation versus continuous IR time. **a** ATM* (red) increase against the decreasing of ATM dimmer (blue) and ATM monomer (green) under the cooperation of DSBCs (black) and positive self-feedback of ATM*; **b** ATM* (blue) reaches saturation after IR overpass 0.5 Gy

(a)

The kinetics of p53*, Mdm2, and ATM* within 800 minutes

The phase difference of oscillations
between p53* and MDM2 is about 100 minutes

(b)

The kinetics of p53-Mdm2 feedback loop under IR = 8Gy

(c)

The kinetics of p53-Mdm2 feedback loop under IR = 2Gy

Fig. 7. The kinetics of p53-MDM2 feedback loop module under continuous IR. **a** Under regulations of ATM* (red), the responses of p53 (blue), and Mdm2 (green) stimulated by 8-Gy IR with oscillations. **b** The whole dynamics of p53-MDM2 feedback loop, more pulses occur versus continuing IR time, and trend to a new equilibrium. **c** The kinetics of p53-MDM2 feedback loop under IR $= 2$ Gy with fewer oscillations and smaller amplitude

3.3 Kinetics of p53-MDM2 feedback loop

The p53-MDM2 feedback loop is a vital part in controlling the downstream genes and regulation pathways to fight against the genome stresses (Lev Bar-Or et al., 2000; Ritter et al., 2002; Weller, 1998). In response to the input signal of ATM^*, the p53-Mdm2 module generates one or more oscillations. The response traces of p53 and Mdm2 protein under continuous application of 8-Gy IR from time 0 are shown in Fig. 7a. Upon the activation by ATM^* and decreased degradation by Mdm2, the total amount of p53 proteins increases quickly. Due to the p53-dependent induction of Mdm2 transcription, the increase of Mdm2 proteins is sufficiently large to lower the p53 level, which in turn reduces the amount of the Mdm2 proteins. The oscillation pulses shown in Fig. 7a have a period of 400 min, and the phase difference between p53 and Mdm2 is about 100 min. Moreover, the first pulse is slightly higher than the second, quite similar with the experimental observations (Ma et al., 2005) and the simulation results (Lahav et al., 2004).

By comparing the results in Fig. 7b and c, we can see that two or more pulses of p53 and MDM2 are generated after increasing the IR doses. Our simulations are fully in accordance with the observations that, in average, the greater the number of p53 pulses, the more severe damage that can be triggered (Lev Bar-Or et al., 2000; Ritter et al., 2002; Weller, 1998). These results show that our model of p53 stress response network yields roughly equal-sized pulses with a mean number that increases with the IR strength and the continuous IR time.

4. Discussion and conclusion

A set of differential equations, combined with the Poisson random function, were proposed to model the DSBs generation and repair process. It is demonstrated according to our model that ATM exhibits a strong sensitivity and switch-like behaviour in response to the number of DSBs, fully consistent with the necessary outcome to transfer the stress signal to the p53-MDM2 feedback loop and arrest the cell cycle in response to the acute IR (Ma et al., 2005). Once the IR dose is sufficiently large, the p53-MDM2 feedback loop will produce oscillations. Especially, the number and amplitude of the oscillations are different according to the cell types and the IR dose domains (Ma et al., 2005). Our mode, although simplified, does provide a framework for the theoretical analysis of the mechanisms of p53 stress response networks in response to continuous IR.

References

Althaus IW, Chou JJ, Gonzales AJ, Diebel MR, Chou KC, Kezdy FJ, Romero DL, Aristoff PA, Tarpley WG, Reusser F (1993a) Steady-state kinetic studies with the non-nucleoside HIV-1 reverse transcriptase inhibitor U-87201E. J Biol Chem 268: 6119–6124

Althaus IW, Gonzales AJ, Chou JJ, Diebel MR, Chou KC, Kezdy FJ, Romero DL, Aristoff PA, Tarpley WG, Reusser F (1993b) The quinoline U-78036 is a potent inhibitor of HIV-1 reverse transcriptase. J Biol Chem 268: 14875–14880

Bakkenist CJ, Kastan MB (2003) DNA damage activates ATM through intermolecular autophosphorylation and dimer dissociation. Nature 421: 499–506

Budman J, Chu G (2005) Processing of DNA for nonhomologous end-joining by cell-free extract. Embo J 24: 849–860

Chou JJ, Li H, Salvessen GS, Yuan J, Wagner G (1999a) Solution structure of BID, an intracellular amplifier of apoptotic signalling. Cell 96: 615–624

Chou KC (1984) Low-frequency vibration of DNA molecules. Biochem J 221: 27–31

Chou KC (1987) The biological functions of low-frequency phonons: 6. A possible dynamic mechanism of allosteric transition in antibody molecules. Biopolymers 26: 285–295

Chou KC (1988) Review: Low-frequency collective motion in biomacromolecules and its biological functions. Biophys Chem 30: 3–48

Chou KC (1989a) Graphical rules in steady and non-steady enzyme kinetics. J Biol Chem 264: 12074–12079

Chou KC (1989b) Low-frequency resonance and cooperativity of hemoglobin. Trends Biochem Sci 14: 212

Chou KC (1990) Review: Applications of graph theory to enzyme kinetics and protein folding kinetics. Steady and non-steady state systems. Biophys Chem 35: 1–24

Chou KC (2004) Review: Structural bioinformatics and its impact to biomedical science. Curr Med Chem 11: 2105–2134

Chou KC, Chen NY (1977) The biological functions of low-frequency phonons. Sci Sin 20: 447–457

Chou KC, Forsen S (1980) Graphical rules for enzyme-catalyzed rate laws. Biochem J 187: 829–835

Chou KC, Jiang SP (1974) Studies on the rate of diffusion-controlled reactions of enzymes. Sci Sin 17: 664–680

Chou KC, Jiang SP, Liu WM, Fee CH (1979) Graph theory of enzyme kinetics: 1. Steady-state reaction system. Sci Sin 22: 341–358

Chou KC, Jones D, Heinrikson RL (1997) Prediction of the tertiary structure and substrate binding site of caspase-8. FEBS Lett 419: 49–54

Chou KC, Kezdy FJ, Reusser F (1994a) Review: steady-state inhibition kinetics of processive nucleic acid polymerases and nucleases. Anal Biochem 221: 217–230

Chou KC, Maggiora GM, Mao B (1989) Quasi-continuum models of twist-like and accordion-like low-frequency motions in DNA. Biophys J 56: 295–305

Chou KC, Mao B (1988) Collective motion in DNA and its role in drug intercalation. Biopolymers 27: 1795–1815

Chou KC, Tomasselli AG, Heinrikson RL (2000) Prediction of the tertiary structure of a caspase-9/inhibitor complex. FEBS Lett 470: 249–256

Chou KC, Watenpaugh KD, Heinrikson RL (1999b) A model of the complex between cyclin-dependent kinase 5(Cdk5) and the activation domain of neuronal Cdk5 activator. Biochem Biophys Res Commun 259: 420–428

Chou KC, Zhang CT (1992) Diagrammatization of codon usage in 339 HIV proteins and its biological implication. AIDS Res Hum Retroviruses 8: 1967–1976

Chou KC, Zhang CT, Maggiora GM (1994b) Solitary wave dynamics as a mechanism for explaining the internal motion during microtubule growth. Biopolymers 34: 143–153

Chou KC, Zhou GP (1982) Role of the protein outside active site on the diffusion-controlled reaction of enzyme. J Am Chem Soc 104: 1409–1413

Cotes NJ, Sceats MG (1988) Biomolecular reactions with a reactive site on a spherical particle: a Hamiltonian formulation. J Chem Phys 89: 2816–2821

Daboussi F, Dumay A, Delacote F, Lopez BS (2002) DNA double-strand break repair signalling: the case of RAD51 post-translational regulation. Cell Signal 14: 969–975

Gao L, Ding YS, Dai H, Shao SH, Huang ZD, Chou KC (2006) A novel fingerprint map for detecting SARS-CoV. J Pharm Biomed Anal 41: 246–250

Han WG (1992) The influence of dipole-dipole interaction on the low-frequency vibrations in alpha-helix proteins. Biophys Chem 43: 169–173

Han WG, Wang CD (1992) The vibrational normal modes of beta-barrels in an IgG antibody molecule. Biophys Chem 44: 29–45

King EL, Altman C (1956) A schematic method of deriving the rate laws for enzyme-catalyzed reactions. J Phys Chem 60: 1375–1378

Kohn KW, Pommier Y (2005) Molecular interaction map of the p53 and Mdm2 logic elements, which control the Off-On switch of p53 in response to DNA damage. Biochem Biophys Res Commun 331: 816–827

Kuzmic P, Ng KY, Heath TD (1992) Mixtures of tight-binding enzyme inhibitors. Kinetic analysis by a recursive rate equation. Anal Biochem 200: 68–73

Lahav G, Rosenfeld N, Sigal A, Geva-Zatorsky N, Levine AJ, Elowitz MB, Alon U (2004) Dynamics of the p53-Mdm2 feedback loop in individual cells. Nat Genet 36: 147–150

Lev Bar-Or R, Maya R, Segel LA, Alon U, Levine AJ, Oren M (2000) Generation of oscillations by the p53-Mdm2 feedback loop: a theoretical and experimental study. Proc Natl Acad Sci USA 97: 11250–11255

Lin SX, Neet KE (1990) Demonstration of a slow conformational change in liver glucokinase by fluorescence spectroscopy. J Biol Chem 265: 9670–9675

Ma L, Wagner J, Rice JJ, Hu W, Levine AJ, Stolovitzky GA (2005) A plausible model for the digital response of p53 to DNA damage. Proc Natl Acad Sci USA 102: 14266–14271

Magne N, Toillon RA, Bottero V, Didelot C, Houtte PV, Gerard JP, Peyron JF (2006) NF-kappaB modulation and ionizing radiation: mechanisms and future directions for cancer treatment. Cancer Lett 231: 158–168

Martel P (1992) Biophysical aspects of neutron scattering from vibrational modes of proteins. Prog Biophys Mol Biol 57: 129–179

Oren M (2003) Decision making by p53: life, death and cancer. Cell Death Differ 10: 431–442

Pauklin S, Kristjuhan A, Maimets T, Jaks V (2005) ARF and ATM/ATR cooperate in p53-mediated apoptosis upon oncogenic stress. Biochem Biophys Res Commun 334: 386–394

Perez CA, Purdy JA (1998) Treatment planning in radiation oncology and impact on outcome of therapy. Rays 23: 385–426

Rapp A, Greulich KO (2004) After double-strand break induction by UV-A, homologous recombination and nonhomologous end joining cooperate at the same DSB if both systems are available. J Cell Sci 117: 4935–4945

Ritter MA, Gilchrist KW, Voytovich M, Chappell RJ, Verhoven BM (2002) The role of p53 in radiation therapy outcomes for favorable-to-intermediate-risk prostate cancer. Int J Radiat Oncol Biol Phys 53: 574–580

Rothkamm K, Kruger I, Thompson LH, Lobrich M (2003) Pathways of DNA double-strand break repair during the mammalian cell cycle. Mol Cell Biol 23: 5706–5715

Sinkala Z (2006) Soliton/exciton transport in proteins. J Theor Biol 241: 919–927

Sobell HM, Banerjee A, Lozansky ED, Zhou GP, Chou KC (1983) The role of low-frequency (acoustic) phonons in determining the premelting and melting behaviors of DNA. In: Clementi E, Sarma RH (eds) Structure and dynamics: nucleic acids and proteins. New York, pp 181–195

Tyson JJ (1999) Models of cell cycle control in eukaryotes. J Biotechnol 71: 239–244

Tyson JJ, Novak B (2001) Regulation of the eukaryotic cell cycle: molecular antagonism, hysteresis, and irreversible transitions. J Theor Biol 210: 249–263

Vogelstein B, Lane D, Levine AJ (2000) Surfing the p53 network. Nature 408: 307–310

Wang M, Yao JS, Huang ZD, Xu ZJ, Liu GP, Zhao HY, Wang XY, Yang J, Zhu YS, Chou KC (2005) A new nucleotide-composition based fingerprint of SARS-CoV with visualization analysis. Med Chem 1: 39–47

Weller M (1998) Predicting response to cancer chemotherapy: the role of p53. Cell Tissue Res 292: 435–445

Xiao X, Shao S, Ding Y, Huang Z, Chen X, Chou KC (2005) An application of gene comparative image for predicting the effect on replication ratio by HBV virus gene missense mutation. J Theor Biol 235: 555–565

Xiao X, Shao SH, Chou KC (2006) A probability cellular automaton model for hepatitis B viral infections. Biochem Biophys Res Commun 342: 605–610

Zhang CT, Chou KC (1994) Analysis of codon usage in 1562 E. Coli protein coding sequences. J Mol Biol 238: 1–8

Zhang CT, Chou KC (1996) An analysis of base frequencies in the anti-sense strands corresponding to the 180 human protein coding sequences. Amino Acids 10: 253–262

Zhou G, Wong MT, Zhou GQ (1983) Diffusion-controlled reactions of enzymes. An approximate analytic solution of Chou's model. Biophys Chem 18: 125–132

Zhou GP (1989) Biological functions of soliton and extra electron motion in DNA structure. Phys Scripta 40: 698–701

Zhou GP, Deng MH (1984) An extension of Chou's graphical rules for deriving enzyme kinetic equations to system involving parallel reaction pathways. Biochem J 222: 169–176

Zhou GQ, Zhong WZ (1982) Diffusion-controlled reactions of enzymes. A comparison between Chou's model and Alberty-Hammes-Eigen's model. Eur J Biochem 128: 383–387

Authors' addresses: J.-P. Qi, Bioinformatics Research Center, Donghua University, Shanghai 200051, China; or G.-P. Zhou, Department of Biological Chemistry and Molecular Pharmacology, Harvard Medical School, Boston, MA 02115, U.S.A.,

E-mail: gzhou@crystal.harvard.edu